

REST HF-10 Test Case: Numerical Simulation of a Single Coaxial LOX-CH₄ Injector with Forced Mass Flow Oscillations Using the DLR TAU-Code

Tim Horchler[†] and Stefan Fechter
German Aerospace Center (DLR)
Institute of Aerodynamics and Flow Technology, Spacecraft Department
Bunsenstr. 10, 37073 Göttingen, Germany
[†]tim.horchler@dlr.de

Jan van Schyndel and Michael Oswald
German Aerospace Center (DLR)
Institute of Space Propulsion, Rocket Propulsion Department
Lampoldshausen, 74239 Hardthausen, Germany

Abstract

Combustion instabilities are high-pressure acoustic oscillations that often develop spontaneously and may lead to catastrophic failure of a liquid rocket engine. In order to investigate this phenomenon, the Rocket Engine Stability initiative (REST) was founded by CNES, ONERA, DLR and CNRS. Supporting current and future engine developments, the REST community has worked towards a better understanding of high-frequency instability phenomena. The advancement of numerical simulation methods created new opportunities to simulate combustion instabilities and allowed for a deeper understanding of processes in rocket engines that are difficult to observe experimentally. Numerical simulations were used to investigate the coupling between different internal processes like pressure oscillations and heat release fluctuations. With Prometheus as the engine of a future European launcher vehicle, predicting instabilities and flame dynamics in methane-oxygen (CH₄-O₂) combustion became an important step in developing reliable, efficient and reusable rocket engines. In order to support these developments numerically, the REST community proposed a representative single injector test case designed for fundamental research. The test case consists of a hexagonal combustion chamber with periodic boundary conditions and a representative injector geometry. The injector was designed within the frame of the "Sonderforschungsbereich Transregio 40", a research program founded by the German Research Foundation (DFG), and is intended to be suitable both for LOx-CH₄ and LOx-H₂ rocket engines. The chamber pressure is set to be 100 bar and instabilities are introduced by modulating the inlet mass flows for methane and the oxygen injector up to $\pm 10\%$ of their nominal values at different frequencies. The main goal of this test case is to compare the different numerical codes and modeling approaches (different turbulence modeling, different combustion modeling) between the members of the REST community and various codes. This paper presents the current status of the DLR contribution to the test case. All simulations are conducted with the DLR in-house Code TAU. The combustion is modeled using a real-gas flamelet model whereas the turbulence is modeled using a 2-layer k- ϵ RANS model. In addition to the URANS simulations, Detached-Eddy simulation (DES) results for all test case load points are presented and compared to the URANS results. It is shown that the URANS simulations greatly overestimates the dense LOx core lengths while the DES results give more reasonable values. Investigations of the flame response to the longitudinal mass flux oscillations showed only a small effect for an excitation of the O₂ inflow at 5 kHz while there is a stronger flame response for the other excited cases. We also present results for numerical grid resolution sensor and a grid convergence study indicating that the chosen mesh resolution allows for grid-converged results for this test case.

1. Introduction

Combustion instabilities in rocket engines have been a major engineering problem since the beginning of the space-age in the 1950's. They are strong unwanted acoustic disturbances that often form spontaneously, and can lead to complete destruction of the rocket engine in a very short time. Even though a lot of research activities⁴ have been devoted to understand and avoid combustion instabilities, no complete theory is available yet and the problem is still not completely solved. One obstacle preventing a better understanding of combustion instabilities is the harsh environment in rocket thrust chambers. High pressures (over 60 bar even for small-scale experimental chambers) and high temperatures, due to chemical reactions, make it difficult to employ optical measurement techniques to learn more about the flow field structure and mechanisms that are involved in the development of combustion instabilities. Even measurements of the chamber wall pressure or the wall heat fluxes are difficult as proper cooling of the measurement elements and the chamber itself must be guaranteed at all times.

Because of the inherent difficulties to investigate flow fields in rocket thrust chambers experimentally, numerical simulations are a promising alternative to better understand how combustion instabilities develop and which key parameters (e.g. fuel or oxidizer temperatures, injector shape and length, positioning of the injectors, etc.) influence the stability behavior. Even more than in the early days of steady state CFD simulations, modern scale resolving simulation techniques like large-eddy simulations (LES) or detached-eddy simulations (DES), along with high-performance computing architectures, allow for detailed investigations of combustion chamber configurations. Even though a lot of progress has been made in the last years, the simulation of a complete flight engine including the thrust chamber, the cooling channels and the fuel/oxidizer manifold system is still very difficult due to the complexity of the problem. But also for small-scale experimental engines, modeling of the various physical mechanisms poses a significant challenge due to the lack of validation data.

The absence of validation data is of course related to the experimental difficulties of observing flames in combustion chambers under realistic conditions, but apart from this, it is also very difficult to investigate many mechanism in an idealized setup under controlled conditions. For the development of combustion instabilities, many physical mechanisms must interact until a large pressure wave forms: The arguably most relevant ones are acoustic waves, heat release from chemical reaction, fluid dynamical phenomena, like e.g. coherent vortex shedding, and thermodynamic effects due to the high pressures inside the chamber. Others, like fluid droplets and surface tension effects are excluded here as only super-critical injection will be considered.

Some effects are easier to validate than others. For example, the acoustic eigenmode shapes of a combustion chamber can be inferred from the results of steady RANS simulations³ or virtual bombing tests.⁵ Validation results for various chemical kinetic schemes are available from many studies of flames (see e.g. results of workshop on turbulent non-premixed flames TNF²). Fluid-dynamical effects related to combustion instabilities have been reviewed by Armbruster,¹ although most of these effects have only been investigated at lower pressures than typically found in rocket thrust chambers. Thermodynamic effects due to the high pressure are also difficult to investigate as there are only few experiments available in the literature. One example is the work of Mayer et al.¹² where the breakup of a supercritical nitrogen jet is investigated experimentally.

A fundamentally different approach for validation has been adopted by Ruiz et al. in their work on a "Numerical benchmark for high-Reynolds-number supercritical flows with large density gradients".¹⁷ The authors proposed a simplified 2D test case for a typical coaxial injection element under representative engine conditions and compared the results for different CFD codes. In the opinion of the authors, this test case is highly useful for two reasons: First, the simplicity of the 2D geometry allows for quick results at a low computational cost. Another reason is the ability to compare modeling aspects (chemical reactions, thermodynamics, etc.) in various codes under representative conditions while not having to deal with complex flow situations. It is even possible to compare simulation results that have been obtained on identical meshes. But this simplicity comes at the price of a unrealistic turbulence field which can not be modeled correctly in 2D simulations.

In order to increase the modeling complexity one step further, the *Rocket Engine Stability Initiative* (REST) developed a single coaxial injector test case inspired by the approach of Ruiz et al., called HF-10. This test case uses a single-injector element developed by the "Sonderforschungsbereich Transregio 40", a project funded by the German Research Foundations (DFG), in a hexagonal combustion chamber. The test case investigates the response of a transcritical CH₄/O₂ flame to longitudinal mass flow perturbations imposed at the inlet boundaries. This work presents URANS and DES results for this test case obtained with the DLR TAU code and a flamelet combustion model.

2. Numerical Setup

For the flow simulations in this work we used the DLR TAU code,¹⁸ a second-order compressible cell-centered finite volume solver. TAU uses a low-Ma-number corrected²¹ version of the MAPS+ upwind solver¹⁶ which shows strongly reduced numerical dissipation for high wavenumbers and is therefore suitable for scale-resolving simulations. Time-accurate simulations use a Jameson-type dual timestepping scheme⁷ with a physical time-step size of 5×10^{-7} s. Solution integration in the inner iterations is performed using an explicit Runge-Kutta-scheme which is accelerated by a local time-stepping approach.

URANS simulations presented in this work use a 2-layer k- ϵ model. Scale-resolving DES results use a zonal delayed-detached eddy simulation (DDES) model¹⁹. This approach treats the first 250 mm of the chamber (including the injector) in DES mode while the rear part near the outflow boundary is treated in URANS mode.

The real-gas properties of fuel and oxidizer at 100 bar chamber pressure are taken into account by using the Soave-Redlich-Kwong cubic equation-of-state.⁹ The species CH₄, O₂ and CO₂ are treated as real gas species while all other species are treated as ideal gas components.

Chemical reactions between fuel (CH₄) and oxidizer (O₂) are simulated with a flamelet combustion model^{13,14} employing the reduced reaction mechanism of Zhukov et al.²²

For the flamelet combustion model, TAU solves additional equations for the mixture fraction \tilde{Z} and the variance of mixture fraction \tilde{Z}''^2 . These parameters, along with the scalar dissipation rate χ , are used to look-up the flame shape from a three-dimensional flamelet table that has been generated in a preprocessing step. Under the assumption that the chemical time scales are much shorter than the turbulent time scales, the flame can locally be approximated by a counter-flow diffusion flame for which a solution can be sought by means of the one-dimensional real-gas flamelet equations.^{6,10}

$$-\rho \frac{\chi}{2} \frac{\partial^2 Y_s}{\partial Z^2} = \dot{m}_s \quad (1)$$

$$-\rho \frac{\chi}{2c_p} \left(\frac{\partial^2 h}{\partial Z^2} - \sum_{s=1}^{N_s} h_s \frac{\partial^2 Y_s}{\partial Z^2} \right) = -\frac{1}{c_p} \sum_s h_s \dot{m}_s \quad (2)$$

Solution to Eqs. 1 and 2 are sought for various values of the stoichiometric scalar dissipation rate χ_{st} , which is a measure of the flame's strain rate. The stoichiometric scalar dissipation rate is used in the profile of the scalar dissipation rate

$$\chi(Z) = \chi_{st} \exp \left[2 \left([\operatorname{erfc}^{-1}(2Z_{st})]^2 - [\operatorname{erfc}^{-1}(2Z)]^2 \right) \right] \quad (3)$$

which is derived under the assumption of a counter-flow diffusion flame.

Based on different solutions of the flamelet equations for values of χ_{st} ranging from $\chi_{st} \approx 0$ 1/s to the quenching point at $\chi_{st} \approx 3 \times 10^5$ 1/s where the flame is extinguished, the flamelet table is created by a convolution integral

$$\bar{Y}_i(\tilde{Z}, \tilde{Z}''^2, \chi) = \int_0^1 \int_0^\infty Y_i(\chi_{st}, Z) P(Z, \tilde{Z}, \tilde{Z}''^2; \chi, \chi_{st}) dZ d\chi_{st}. \quad (4)$$

with the probability density function kernel $P(Z, \tilde{Z}, \tilde{Z}''^2; \chi, \chi_{st})$. Under the assumption of statistical independence of Z and χ , the PDF kernel is split up into a product of separate PDFs. The PDF for the mixture fraction is modeled using a two-parameter beta distribution while the scalar dissipation PDF is modeled using a δ -distribution. The flamelet model uses the exact same thermodynamics as the TAU code. In order to speed up the computation of the cubic coefficients and the gas transport properties, the flamelet table also stores linearized coefficients according to the method of Terrapon et al.²⁰ The full flamelet lookup including \tilde{Z} , \tilde{Z}''^2 and χ is currently only used for the RANS computations. For the DES results, the influence of scalar dissipation rate is neglected and only the near-equilibrium flamelet is used. Similarly, the influence of subgrid-scale turbulence-chemistry interaction is neglected, therefore rendering the flamelet model an essentially infinitely-fast chemistry model. Even though these are strong assumptions that will give an overestimation of the flame temperature, the effect of modeled subgrid-scales on the overall flame will be smaller for DES than for RANS simulations as more of the turbulent flow features are resolved on the grid.

Test case HF-10 consists of a 300 mm long combustion chamber attached to a single recessed coaxial injector (see also Fig. 2). The detailed sizes of the injector and combustion chamber can be found in the HF-10 test case description and are shown in Fig. 1.

The combustion chamber is operated at a chamber pressure (imposed at the exit boundary condition) of 100 bar. Oxygen is injected at 100 K with a mass flow rate of 0.46 kg/s. Methane is injected at room temperature of $T = 231$ K with a mass flow rate of 0.136 kg/s. All physical walls (injector and face plate walls) are modeled using an adiabatic

REST HF-10 TEST CASE: RESULTS WITH THE DLR TAU-CODE

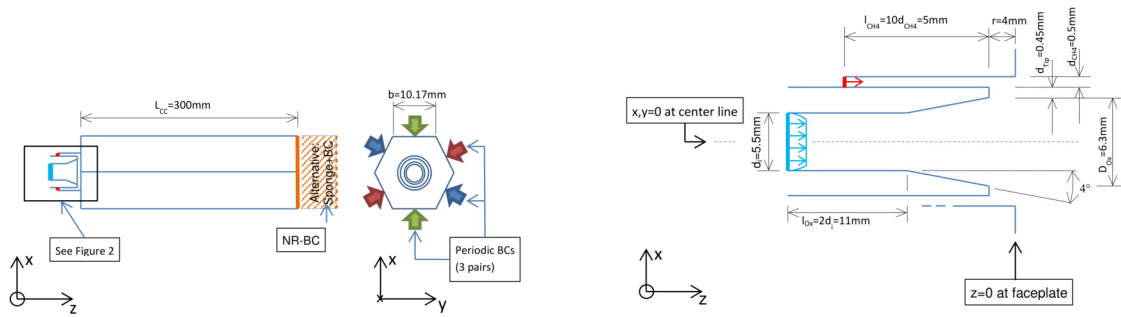


Figure 1: Geometric setup of the testcase. Left: Setup of the whole domain. Right: Size of the coaxial injector.

non-slip wall. The chamber walls on opposing sides in x -direction are modeled using a pair of periodic boundaries while the two other opposing pairs use a symmetry boundary conditions due to a restriction in the TAU code. All inflow boundaries use mass-flux inflow boundary at which the mass flux density and a the static temperature is specified. At the outflow, a subsonic outflow boundary condition is used at which an exit-pressure 100 bar is specified.

Different meshing approaches have been used for the RANS and the DES simulations, see Fig. 2. The RANS mesh (mesh M1, Fig. 2 left) has been created as a hybrid mesh contains in total 3.02 mio. mesh points and consists of hexaeder, tetraeder and pyramids. The DES mesh, however, is a fully block-structured hexaeder mesh consisting of 12.3 mio. mesh points. It will be labeled as M2 in the remainder of this work.

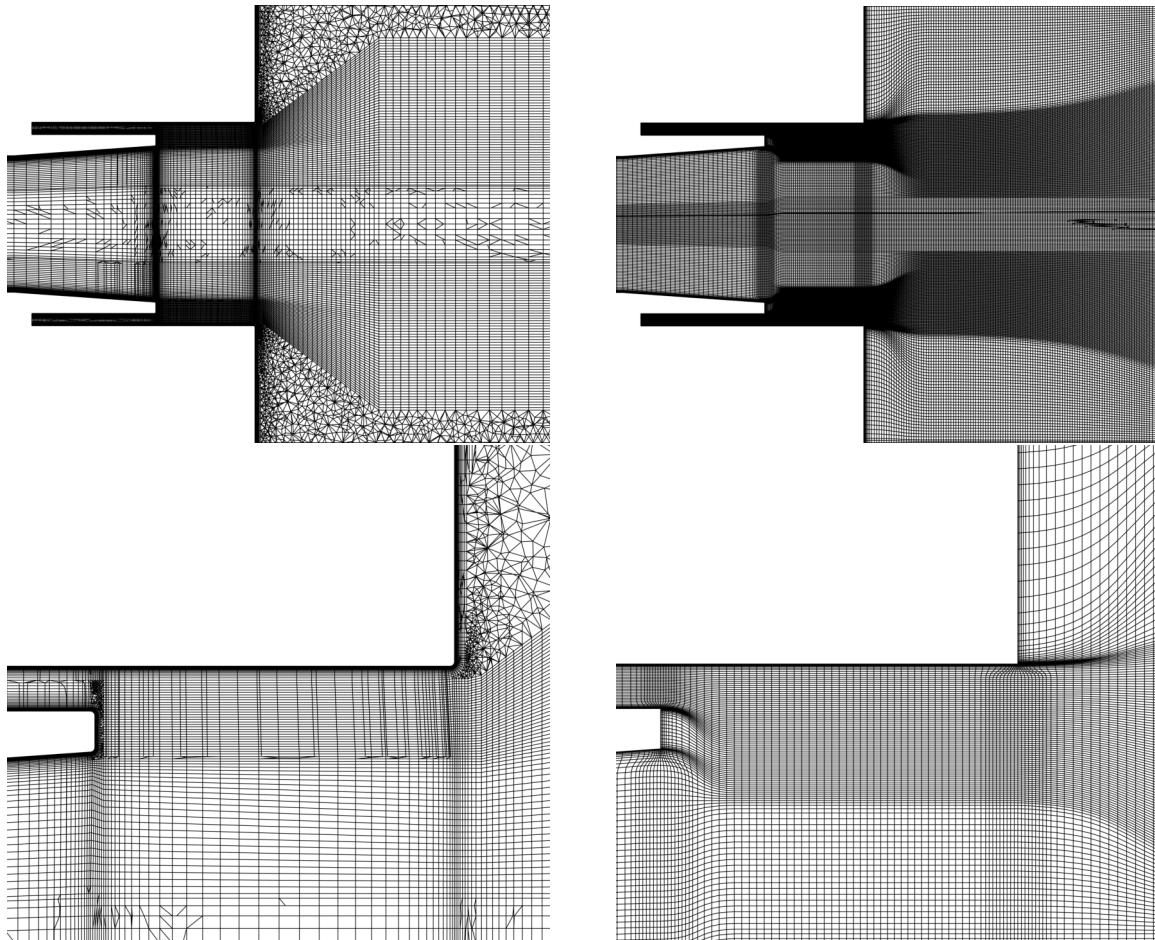


Figure 2: **Left column:** Mesh structure of the hybrid RANS mesh M1. **Right column:** Fully structured hexaeder mesh for the detached-eddy simulations M2.

A comparison of the two meshing approaches are shown in Fig. 2. Both meshes are refined at the recessed injector lip to resolve the development of vortical structures in the shear layer. This initial refinement is then reduced

inside the hexahedral combustion chamber where no special refinement is required after the flame is fully developed.

In order to perform a grid convergence study within this work, a refined version of the structured mesh (not shown) has been generated. This mesh (M3) consists of 43.5 mio. grid points. A comparison of solutions obtained on different meshes will be shown in Sec. 4 of this paper.

3. Simulation Results

In this section, the results from simulations of different load points are presented and discussed. The first subsection compares the steady-state results from a RANS simulation with time-averaged results from the DES without excitation. Apart from differences in the length of the dense oxygen cores, and therefore the flame, the simulation results also indicate deviations in the heat release rate and the flow temperature, which will also be investigated in section.

The later parts of this chapter will investigate the flame response to three different inflow massflux variations of $\pm 10\%$ of the nominal value. For the O_2 inflow excitation at 5 kHz, also URANS results are available, which will be compared to the DES results. For all other excitation conditions, the simulations results will be compared to the time-averaged DES result without excitation.

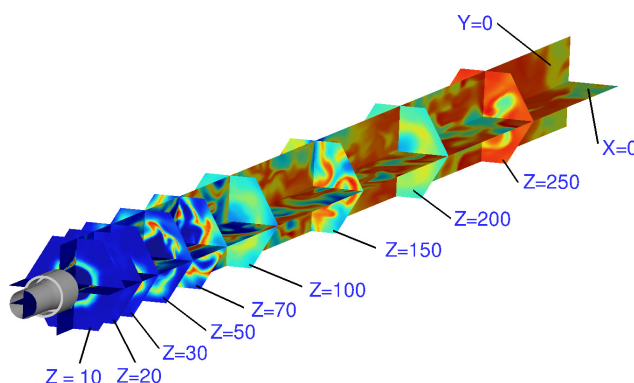


Figure 3: Overview of the different field cuts for HF-10.

We compare the simulation results in this work based on different mesh cuts shown in Fig. 3. All isocontour plots are shown in the $x = 0$ plane, except for mesh convergence results, which are reported in the $y = 0$. Different flow variables are reported in terms of axial line plots. For the axial line plots, weighted averages are calculated on the Z slices shown in Fig. 3. These plots are obtained by averaging all mesh points within a small radial shell of size $\delta A = 2\pi R \cdot \delta R$ and integrating them, weighted by the shell area, in radial direction.

3.1 Steady-State Results

In the first part of the results section, we present the numerical simulation results for the steady-state unexcited condition. This load point serves as the baseline simulation to which the results including mass flow modulation can be compared. Fig. 4 shows the dense oxygen cores for the URANS and the detached-eddy simulation.

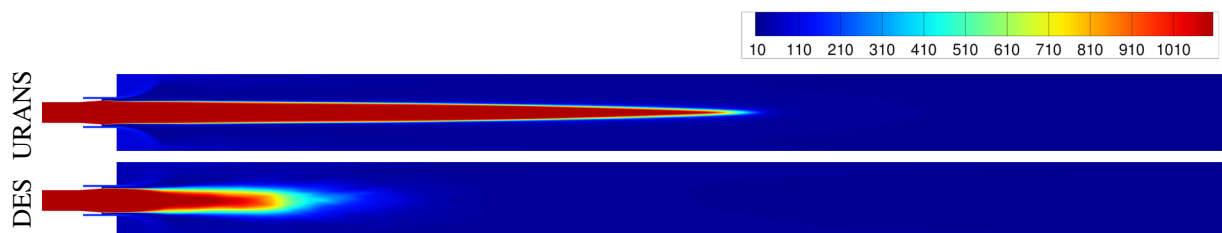


Figure 4: Comparison of the density field in the $x = 0$ plane. The contour values are given in kg/m^3 .

One notices that the URANS simulation shows a largely overestimated LOx core length, which will be seen also in all other URANS results shown in this work. The estimation of LOx core lengths in RANS simulation depends

REST HF-10 TEST CASE: RESULTS WITH THE DLR TAU-CODE

largely on the choice of Schmidt- and Prandtl numbers because the viscous fluxes are dominated by the turbulent eddy viscosity. For example, the heatflux vector in TAU for a flamelet combustion model (Lewis number $Le = 1$) is given by

$$q_i = - \left(\frac{\mu_{lam.}}{Sc_{lam.}} + \frac{\mu_{turb.}}{Sc_{turb.}} \right) \frac{\partial h}{\partial x_i} \quad (5)$$

The situation is different for scale-resolving simulations like DES where most of the turbulent structures are resolved and less turbulence is modelled using a subgrid-scale eddy viscosity. Therefore, the contribution of the second term $\mu_{turb.}/Sc_{turb.}$ is much smaller. The results of the LOx core length also depends on the choice of the turbulence model which directly influences the value of $\mu_{turb.}$.

Now the question arises which of the shown LOx core lengths are more realistic. A preliminary comparison between the results shown here, and results from the last REST (Rocket Engine Stability Initiative) workshop in 2019, suggest that the DES LOx core lengths are more representative. An update of the REST results will be presented by Kaess⁸ in the same conference session as this paper. The result is also confirmed by a comparison to the results of Lechtenberg,¹¹ which will be also presented in this EUCASS conference.

Even though the LOx core (and flame length) in the URANS simulations are not correct, the results are still presented as they allow for a comparison of the temperature field and the heatrelease rate, which are shown in Fig. 5 and Fig. 6, respectively.

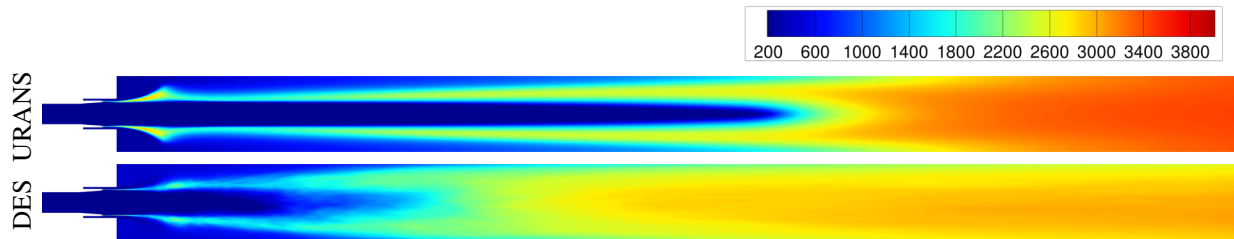


Figure 5: Comparison of the temperature field in the $x = 0$ plane. The contour values are given in K.

Comparing the temperature fields between the URANS and the DES results, we notice that the URANS temperature is much higher near the exit boundary condition, compared to the DES results.

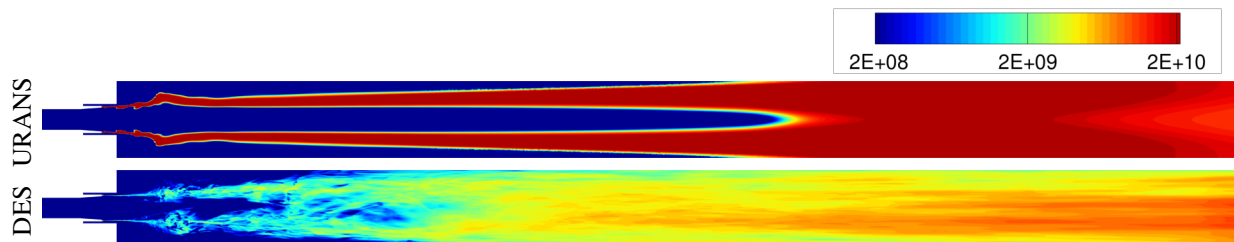


Figure 6: Comparison of the heatrelease field in the $x = 0$ plane. The contour values are given in W/m^3 .

A similar observation can be made in terms of the heatrelease rate, which is about one order of magnitude larger for the URANS simulation in Fig. 6.

The differences between the two modeling approaches can be analyzed more quantitatively by the axial line plots in Fig. 7. Comparing the temperature between URANS and DES indicates an underestimation of about 350 K near the outlet boundary.

Similarly, the heatrelease rate is underestimated, as shown in the graph. The difference in temperature also directly translates into a difference in the axial flow velocity. This test case is operated at a constant pressure, therefore, if the fluid temperature is increased, the density (for a fixed composition) is decreased. The total mass flow rate $\rho u A$ is also constant, therefore, if the density is decreased, the velocity must increase, which explains the differences in axial velocity after $z = 150$ mm.

We argue that the differences in temperature and heatrelease rate between the URANS and the DES results can be attributed to simplifications of the combustion model used in the detached-eddy simulations. Due to limited computing resources and previously good experience with the infinitely fast chemistry model, we decided to employ

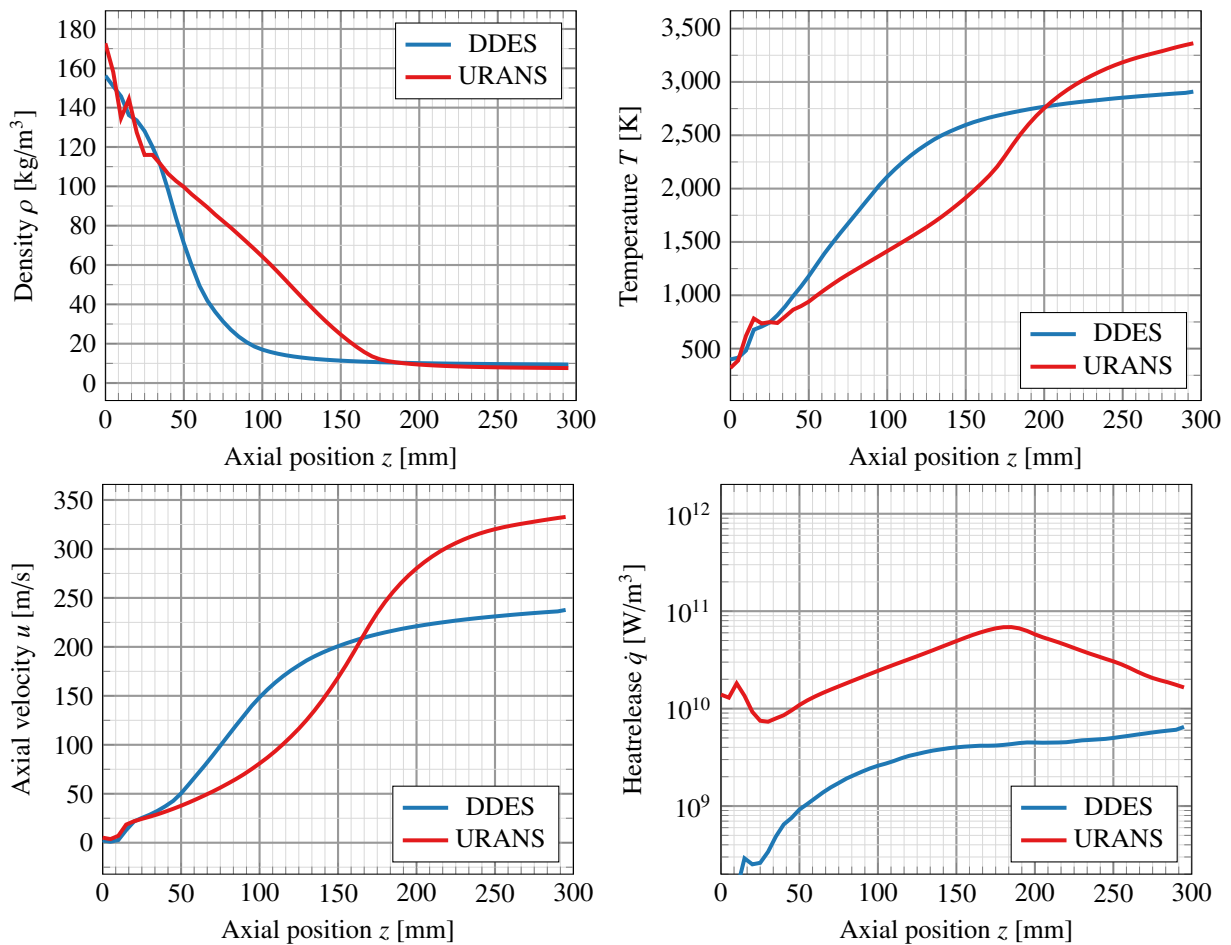
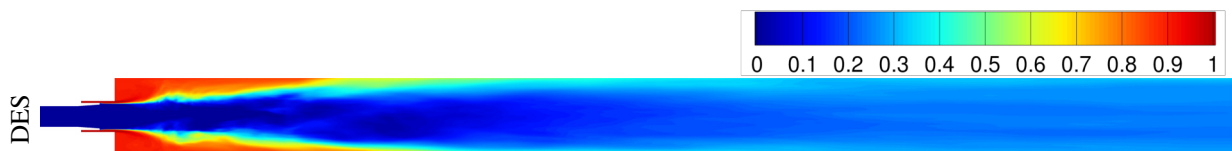


Figure 7: Axial profiles of different flow variables.

only the reduced flamelet model for DES compared to the full flamelet model in the URANS simulation. While for the URANS, the flame state is looked up in the flamelet table based on the mixture fraction Z , the variance of mixture fraction Z''^2 and the scalar dissipation rate χ . For the DES, the lookup is reduced to the mixture fraction, and a near-equilibrium flamelet with $\chi \approx 0$ and $Z''^2 = 0$ is assumed. Fig. 8 shows the steady-state mixture fraction in the chamber.

Figure 8: Comparison of the mixture fraction field in the $x = 0$ plane. The contour values are dimensionless.

The near-exit region is dominated by fluid of $Z \approx 0.3 - 0.4$. When doing the look-up step in the flamelet table, these values of Z result in different temperatures, depending on the scalar dissipation χ , as shown in Fig. 9. One notices the increase in temperatures on the fuel-rich side for higher scalar dissipation rates, which is different to H₂/O₂ simulations where no such effect can be seen. Hence, the URANS model uses the correct value of the scalar dissipation rate and therefore predicts a higher temperature in the near-exit part of the flow field. Similarly, depending on the scalar dissipation rate in the chamber, the URANS model predicts a heat release that is orders of magnitude larger than the DES model.

In summary, this discussion shows that the differences in the temperature field can be attributed to the chosen combustion model for the detached-eddy simulation. Even though the near-injector flame shape and length is reasonable for the DES, the near-exit field shows an underestimation of the temperature. For the URANS, the situation

REST HF-10 TEST CASE: RESULTS WITH THE DLR TAU-CODE

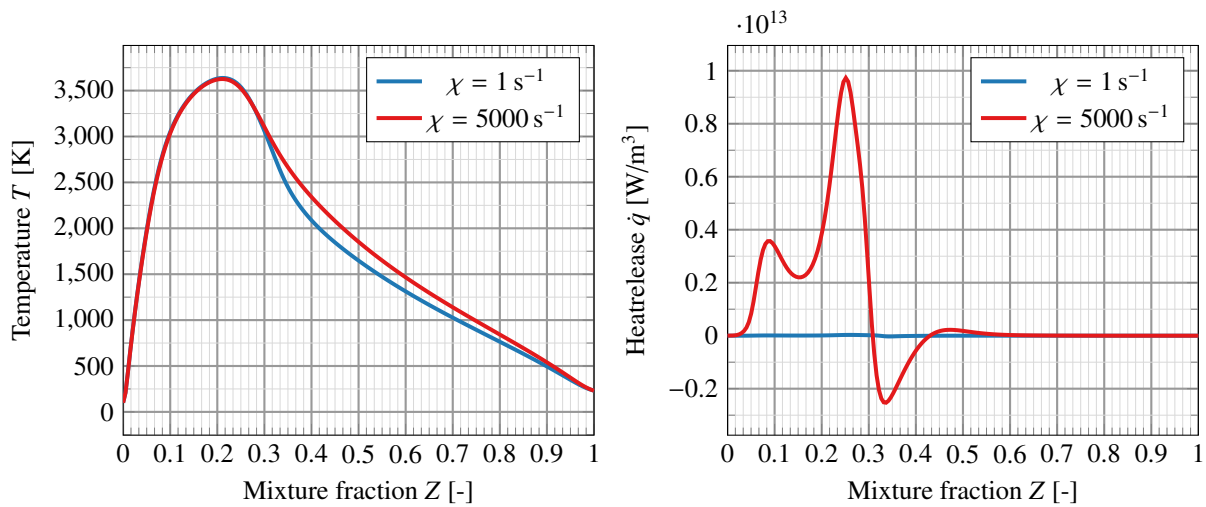


Figure 9: Comparison of two flamelet solutions for different scalar dissipation rates χ .

is reversed: While the near-injector field including the flame shape is incorrect, the overall combustion modeling is correct and gives a reasonable temperature and heatrelease field, but at the wrong location.

3.2 Excitation of the O₂ inflow at 5 kHz

The next set of results shows the same testcase, but with an mass flow excitation of 10 % at the O₂ inlet. For this load point, results for URANS, DES and the steady DES are compared, as shown in Fig. 10 and Fig. 11.

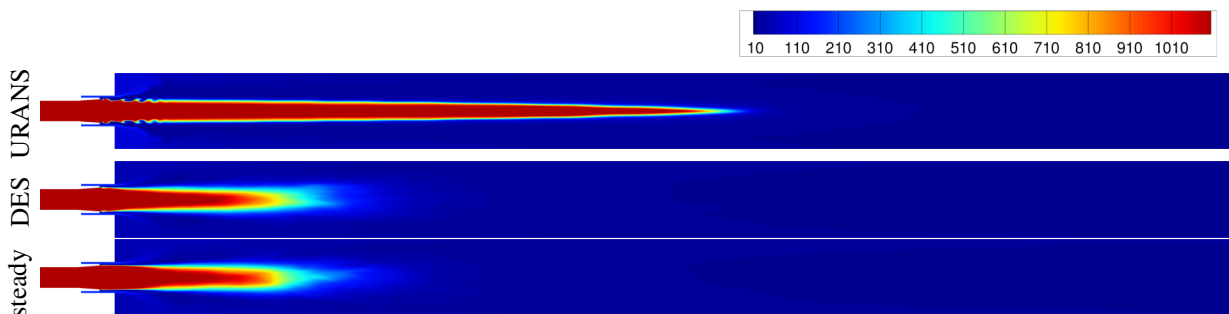


Figure 10: Comparison of the density field in the $x = 0$ plane. The contour values are given in kg/m^3 .

The resulting temperature and density fields only show a very weak influence of the mass flux oscillation on the overall flame shape. Compared to the steady DES results, the length of the LOx core is slightly reduced which is best seen in the axial line plots Fig. 12. The influence of the unsteady mass flow oscillation at the O₂ inlet can be seen as small ripples in the URANS results. These ripples, however, are strongly damped and dissipate as they travel downstream along the interface of the dense LOx core.

Similarly, only small changes are seen in the mean temperature field, Fig. 11. The overall flame shape remains the same, but one notices a significantly thicker flame shoulder compared to the steady DES.

Comparing the axial line plots shows a larger influence of the mass flow modulation for the URANS simulation than for the DES. The largest effect is seen for the axial velocity, which is decreased by about 25 m/s compared to the steady results (dashed line).

It is interesting to note that the largest effect on the heat release for the detached-eddy simulation is confined to the first 40 mm of the combustion chamber. This indicates that the effect of the mass flow oscillation is limited to only a small region near the face plate. This is different from the other excitation conditions, where oscillating mass flux reaches further into the combustion chamber. We conclude on the results of the 5 kHz O₂ oscillations that there is only a very small effect on the overall flame shape for the detached-eddy simulation.

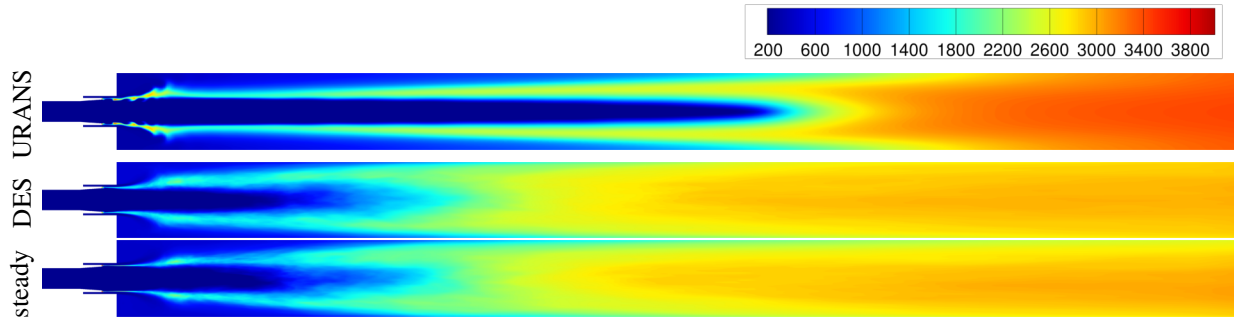


Figure 11: Comparison of the density field in the $x = 0$ plane. The contour values are given in kg/m^3 .

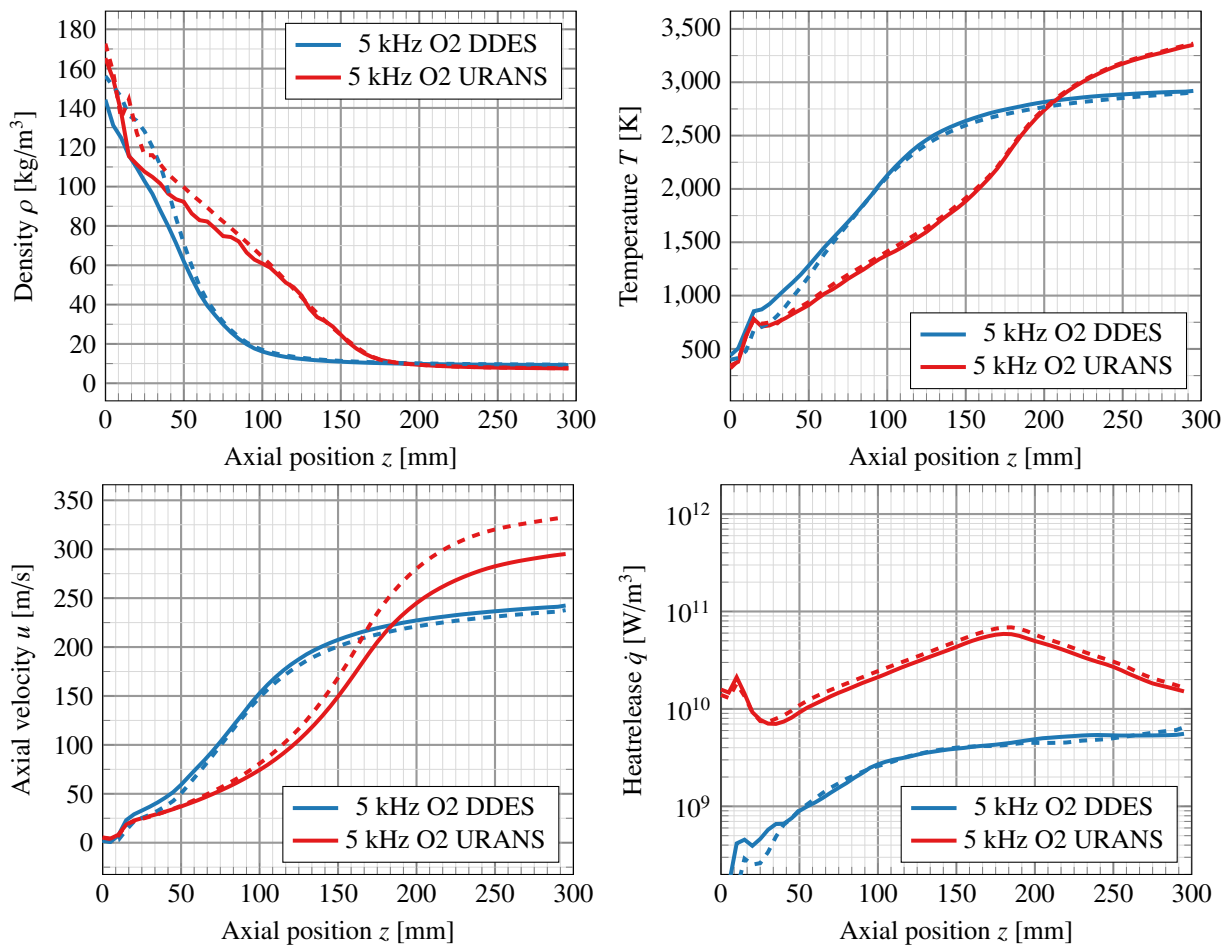


Figure 12: Axial line plots for different flow variables. The dashed lines refer to the steady-state simulation results without mass flow modulation.

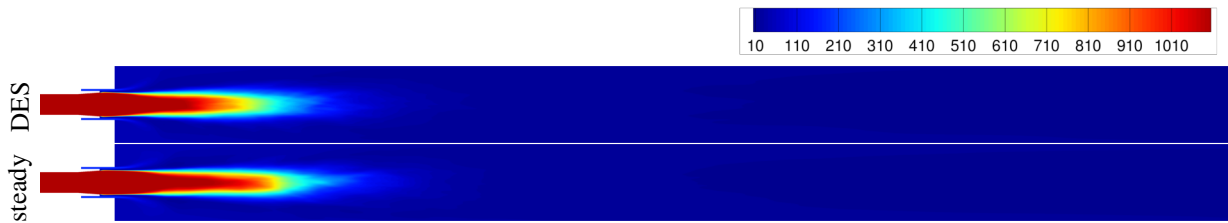
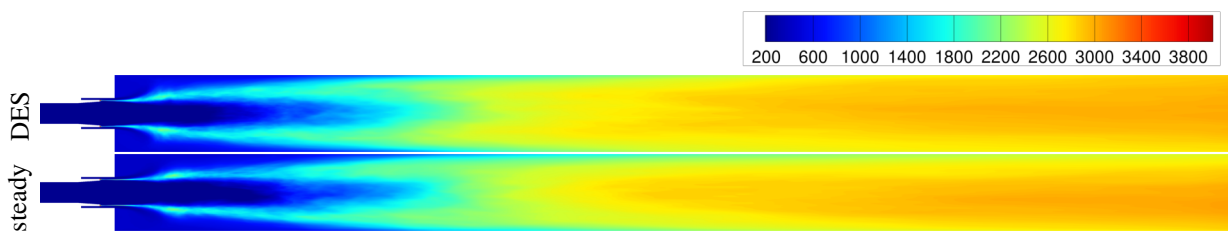
3.3 Excitation of the CH_4 inflow at 5 kHz

Compared to the 5 kHz mass flow modulation at the O_2 inlet, a modulation of the CH_4 fuel mass flow rate resulted in a significant reduction of the flame length, as seen in Fig. 13 and 14.

These results show that the mass flow oscillations leads to a fast consumption of the dense oxygen core and therefore to a shorter flame, as indicated by the temperature field.

This interpretation is also supported by the axial profiles, Fig. 15. These plots show that the flow temperature increases compared to the steady-state solution, therefore giving a lower density (at constant pressure) near the outflow boundary. This results in a higher axial velocity caused by the constant mass flow rate in the test case. Likewise, the

REST HF-10 TEST CASE: RESULTS WITH THE DLR TAU-CODE

Figure 13: Comparison of the density field in the $x = 0$ plane. The contour values are given in kg/m^3 .Figure 14: Comparison of the density field in the $x = 0$ plane. The contour values are given in kg/m^3 .

heat release rate is increased compared to the steady case which explains the higher temperature of the flow.

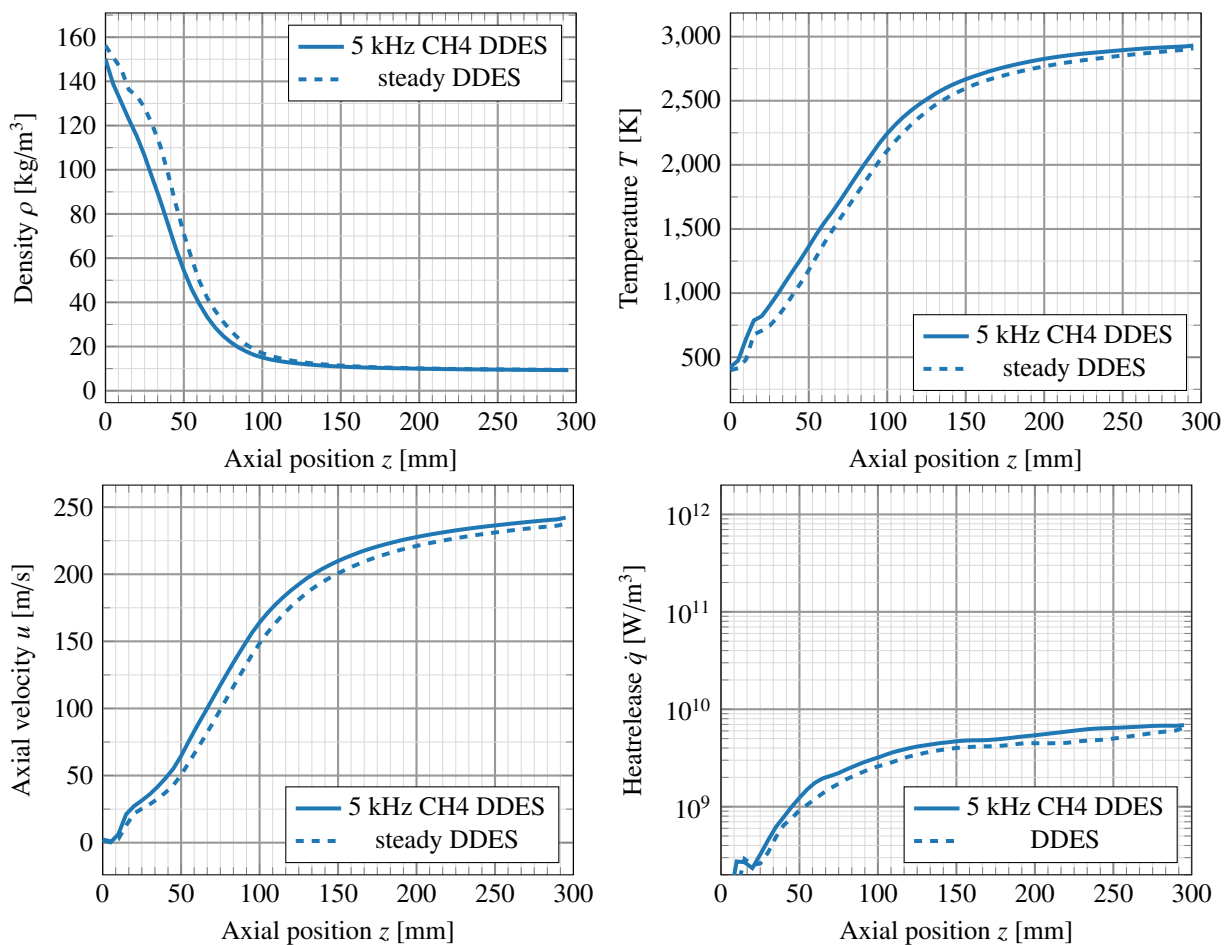


Figure 15: Axial line plots for different flow variables. The dashed lines refer to the steady-state simulation results without mass flow modulation.

3.4 Excitation of the O₂ inflow at 1 kHz

The last load point under investigation is a 1 kHz mass flow oscillation at the O₂ inlet. We omitted the flow field cuts here for brevity as the mean density and temperature field is very similar to the previous results with a 5 kHz CH₄ oscillation. Focusing on the axial line plots in Fig. 16, we notice again the faster consumption of the dense oxygen cores leading to a higher temperature compared to the steady DES.

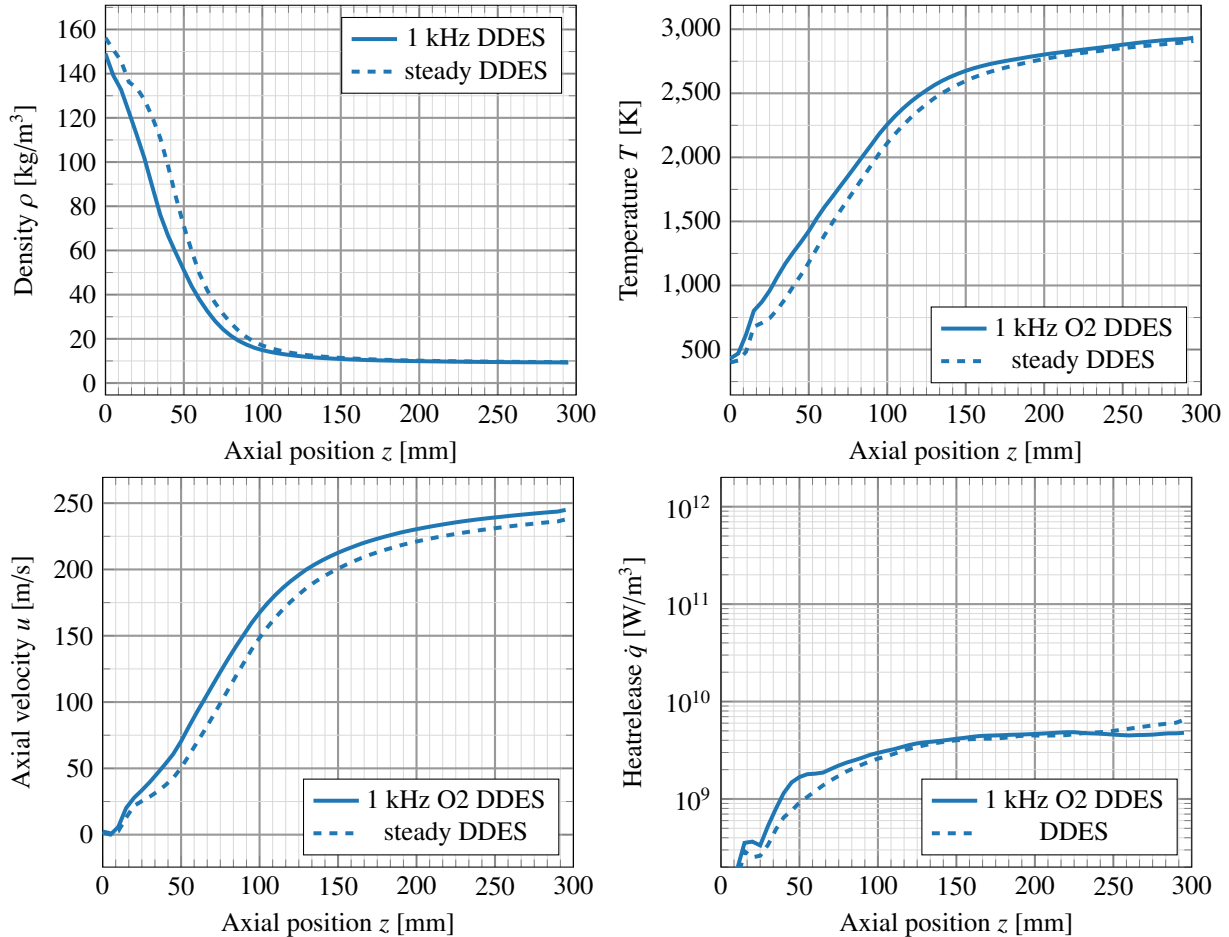


Figure 16: Axial line plots for different flow variables. The dashed lines refer to the steady-state simulation results without mass flow modulation.

In contrast to the excitation at 5 kHz CH₄, we see the highest deviation in flow temperature in the first half of the chamber which then reduces to almost zero near the outflow boundary. As before, the higher temperature results in a higher axial flow velocity, as seen in Fig. 16. The heat release profile shows a pronounced peak at about 40 mm behind the injection plane. A much weaker peak is also visible for the CH₄ modulation results. In light of the previous discussion on the combustion model, this indicates that the mixture fraction field is influenced by the mass flow oscillations therefore changing the mixing state.

4. Assessment of the Mesh Resolution and Grid Convergence Study

The last part of this paper is devoted to a DES grid convergence study for this test case. To this end, the results of three identical detached-eddy simulations with different grids are presented and compared. In order to check for a grid converged solution, we ran the steady-state DES on the RANS mesh (M1, 3.02 mio. points), the standard structured mesh (M2, 12.3 mio. points) and a strongly refined structured mesh (M3, 43.5 mio. points).

In Fig.17, we show the shape of the dense oxygen cores for the three meshes. The overall length of the cores is very similar, with the core length on the RANS mesh being slightly larger than for the structured meshes. But on the RANS mesh, one notices a long density streak artifact that extends into the combustion chamber, which is not seen with the other meshes. This results suggests that the RANS mesh is unsuitable for a DES, as it was expected.

REST HF-10 TEST CASE: RESULTS WITH THE DLR TAU-CODE

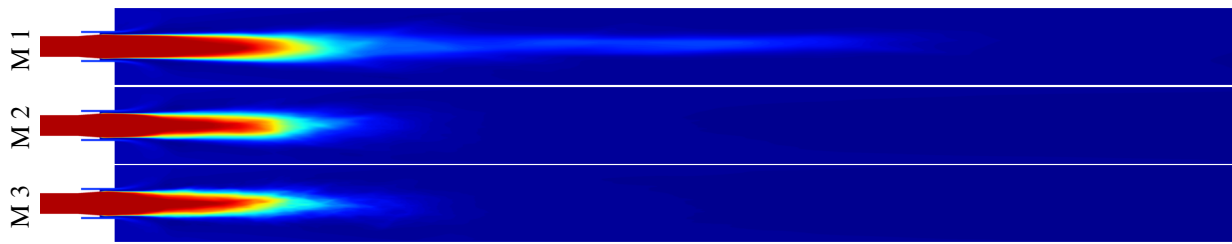


Figure 17: Comparison of the density in the $z = 0$ plane. The contour values are given in kg/m^3 .

DES and URANS require different meshing strategies. Most importantly, meshes for scale-resolving simulations should be isotropic away from solid walls while for RANS meshes, the axial spacing can be largely increased as no vortical structures need to be resolved. It is, however, remarkable that the overall flame shape is well captured on the RANS mesh even with an under resolved DES.

The results for both structured meshes agree very well even though there are small differences in the flame shape visible. In our opinion, these differences are likely related to different averaging lengths of the flow fields, i. e. that both flow fields have been averaged with an unequal number of samples. As the analysis of other variables like temperature and heat release rate showed similar results, we argue that the flow solutions are mesh convergent on the M2 grid, and therefore sufficiently resolved for a DES.

Another method of assessing the grid resolution has been suggest by Reuss et al.¹⁵ In this method, the ratio of resolved turbulent kinetic energy $k_{\text{res.}}$ to the sum of resolved and subgrid-scale turbulent kinetic energy k_{SGS} is evaluated and used as as grid sensor:

$$S_1 = \frac{k_{\text{res.}}}{k_{\text{res.}} + k_{\text{SGS}}} \quad (6)$$

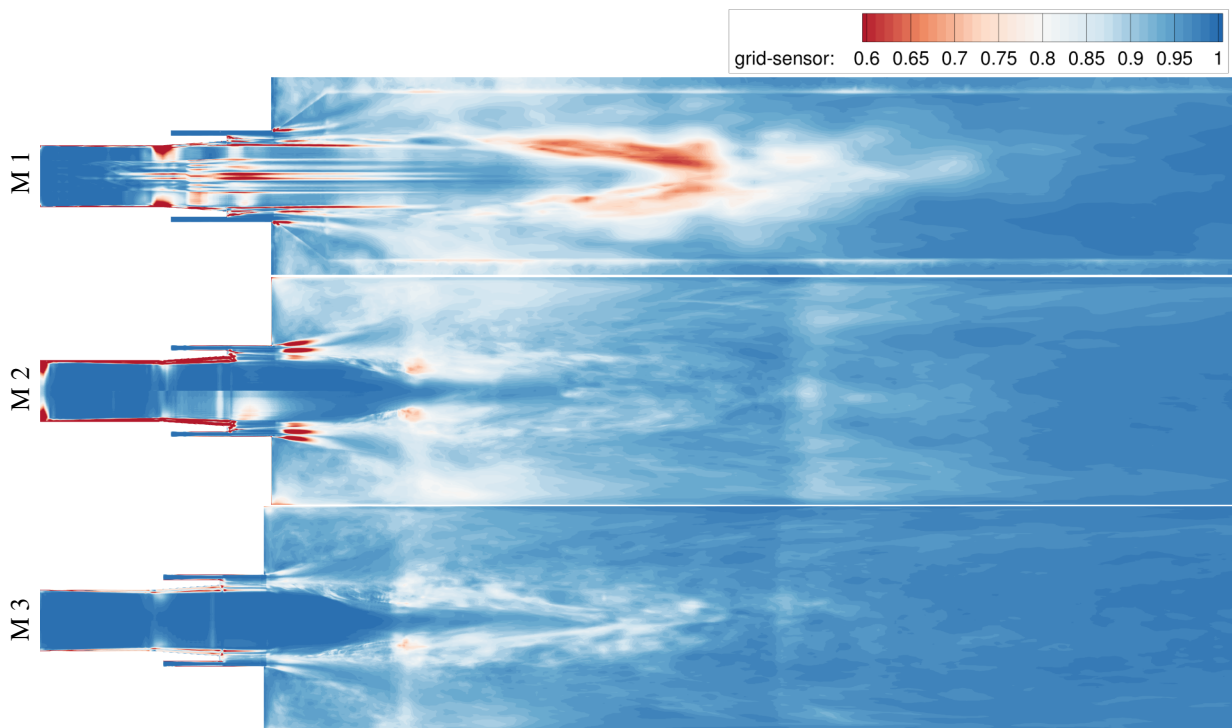


Figure 18: Comparison of the grid sensor in the $y = 0$ plane. The contour values are given in percent.

It is suggested that the flow is well resolved if 80 % of the turbulent kinetic energy are explicitly resolved and only 20 % are modeled. The value of the grid sensor S_1 is shown in Fig. 18 where the color white indicates the threshold of 80 %, and red colors represent an under resolved region. Likewise, blue marks region of higher resolution. Investigating the mesh resolution from the coarsest (M1) to the finest grid (M3) indicates that the RANS mesh is

not sufficiently fine to resolve the full spectrum even within the chamber. The coarse structured mesh (M2) already captures more than 80 % of the kinetic energy inside the chamber even though there two small patches that under resolve the turbulent structures. One also notes two regions in the shear layers inside that chamber where the flow is under resolved. This region is more refined in the very fine structured grid where all regions inside the chamber (downstream of the face plate) are well resolved.

This method shows that most parts of the combustion chamber for the M2 are well resolved agreeing with the observation that the coarse structured mesh resolves most parts of the flow field sufficiently. Compared to a classical mesh convergence study, the grid sensor can be calculated while the computations are running therefore allowing for a simple estimate of the mesh capability to resolve turbulent flow features.

5. Summary and Conclusion

This paper presented an overview of URANS and delayed-detached eddy simulation results for the REST HF-10 testcase that have been obtained with the DLR TAU code. Comparison of the unexcited steady-state results for URANS and DDES indicated that URANS greatly overestimated the length of the dense of LOx core, and therefore the flame. The overall temperature and heat release field is, however, reasonable but is shifted too far downstream. Based on a preliminary comparison with results of other codes, the flame and LOx core length for the DES appears correct. However, the DES shows variations to the URANS model in terms of the temperature field and the heat release. These differences are explained by the choice of the combustion model which neglects the influence of the scalar dissipation rate. Because of this assumption, the temperature on the fuel rich side is lower than expected as it would increase with an increased scalar dissipation rate. The same mechanism also applies to the heat release rate, which is also underestimated in some areas of the flow.

Comparison of simulation results for different excitation load points shows flame responses of varying degrees. For the O₂ excitation at 5 kHz, only a very small shift in the flow field is observed for the DDES. This is in contrast to the simulations with a 5 kHz CH₄ and a 1 kHz O₂ excitation. Here, we observe a stronger effect, especially on the length of the dense oxygen cores and the axial velocity. The overall effect is largest for the 5 kHz CH₄ excitation.

The paper concludes with a grid convergence study for the unexcited steady-state case showing that the standard structured mesh with 12.3 mio. grid points allows for grid-converged results with DDES. It was also shown that even though the RANS mesh clearly under resolves the flow field, the length of the central dense oxygen core is approximately correct and much more reasonable compared to the RANS simulation results.

Another measure of grid resolution is presented in terms of a grid sensor variable indicating how much turbulent kinetic energy is resolved compared to the total turbulent kinetic energy. The results show that most of the flow inside the chamber is already well resolved above 80 % on the standard DES mesh while there are some areas near the shear layers that are still under resolved. Results for the very fine mesh show that the flow is resolved to more than 80 % almost everywhere in the numerical domain.

6. Acknowledgments

The authors appreciate support from the German Aerospace Center (DLR) project AMADEUS (Advanced Methods for Reusable Aerospace Vehicle Design using Artificial Intelligence and Interdisciplinary Numerical Simulation) focusing on the development of numerical methods for LOx-methane-based engine concepts in future space transportation systems. We would also like to thank Ansgar Lechtenberg (DLR) for providing the structured meshes for this study.

References

- [1] Wolfgang Armbruster, Justin Hardi, and Michael Oswald. Impact of shear-coaxial injector hydrodynamics on high-frequency combustion instabilities in a representative cryogenic rocket engine. In *Proceedings of the Symposium on Thermoacoustics in Combustion: Industry meets Academia (SoTiC)*, 2021.
- [2] Robert S. Barlow, editor. *Proceedings of the International Workshop on Measurement and Computation of Turbulent Nonpremixed Flames.*, 1996.
- [3] Scott Kenneth Beinke. *Analyses of Flame Response to Acoustic Forcing in a Rocket Combustor*. Dissertation, School of Mechanical Engineering, The University of Adelaide, Australia, 2017.
- [4] Fred EC Culick and Vigor Yang. Overview of combustion instabilities in liquid propellant rocket engines. *Liquid Rocket Engine Combustion Instability*, 169:3–37, 1995.

REST HF-10 TEST CASE: RESULTS WITH THE DLR TAU-CODE

- [5] Tim Horchler, Stefan Fechter, and Justin Hardi. Numerical investigation of flame-acoustic interaction at resonant and non-resonant conditions in a model combustion chamber. In *Proceedings of the Symposium on Thermoacoustics in Combustion: Industry meets Academia (SoTiC)*, 2021.
- [6] Tim Horchler, Stefan Fechter, Sebastian Karl, and Klaus Hanneman. A timescale-augmented spalart-allmaras turbulence model for flamelet combustion applications. In *8th European Conference for Aeronautics and Aerospace Sciences (EUCASS)*, number 512, 2019.
- [7] Antony Jameson. Time dependent calculations using multigrid, with applications to unsteady flows past airfoils and wings. In *10th Computational Fluid Dynamics Conference*, page 1596, 1991.
- [8] Roland Kaess. Rest hf-10 test case: Synthesis of the contributions for the simulation of excited methane flames under real gas conditions. In *9th European Conference for Aerospace Sciences (EUCASS)*, 2022.
- [9] Seong-Ku Kim, Hwan-Seok Choi, and Yongmo Kim. Thermodynamic modeling based on a generalized cubic equation of state for kerosene/lox rocket combustion. *Combustion and flame*, 159(3):1351–1365, 2012.
- [10] Seong-Ku Kim, Sung-Mo Kang, and Yong-Mo Kim. Flamelet modeling for combustion processes and nox formation in the turbulent nonpremixed co/h₂/n₂ jet flames. *Combustion science and technology*, 168(1):47–83, 2001.
- [11] Ansgar Lechtenberg. Rest hf-10 test case: Flame response to a forced excitation of a methane driven rocket combustion chamber. In *9th European Conference for Aerospace Sciences (EUCASS)*, 2022.
- [12] Wolfgang OH Mayer, Axel HA Schik, Bruno Vielle, Christian Chauveau, Iskender Gokalp, Douglas G Talley, and Rodger D Woodward. Atomization and breakup of cryogenic propellants under high-pressure subcritical and supercritical conditions. *Journal of Propulsion and Power*, 14(5):835–842, 1998.
- [13] Norbert Peters. *Turbulent combustion*. Cambridge university press, 2000.
- [14] Heinz Pitsch. *Entwicklung eines Programmpakets zur Berechnung eindimensionaler Flammen am Beispiel einer Gegenstromdiffusionsflamme*. Diplomarbeit, Rheinisch-Westfälische Technische Hochschule Aachen, 1993.
- [15] Silvia Reuß, T Knopp, A Probst, and M Ortl. Assessment of local les-resolution sensors for hybrid rans/les simulations. In *Progress in Hybrid RANS-LES Modelling*, pages 93–103. Springer, 2015.
- [16] Cord-Christian Rossow. Extension of a compressible code toward the incompressible limit. *AIAA journal*, 41(12):2379–2386, 2003.
- [17] Anthony M Ruiz, Guilhem Lacaze, Joseph C Oefelein, Raphael Mari, Bénédicte Cuenot, Laurent Selle, and Thierry Poinot. Numerical benchmark for high-reynolds-number supercritical flows with large density gradients. *AIAA Journal*, 54(5):1445–1460, 2015.
- [18] D. Schwamborn, T. Gerhold, and R. Heinrich. The DLR-TAU-Code: Recent applications in reasearch and industry. In *Proceedings of the European Conference on Computational Fluid Dynamics (ECCOMAS)*, 2006.
- [19] Philippe R Spalart, Shur Deck, Michael L Shur, Kyle D Squires, M Kh Strelets, and Andrei Travin. A new version of detached-eddy simulation, resistant to ambiguous grid densities. *Theoretical and computational fluid dynamics*, 20(3):181, 2006.
- [20] Vincent Terrapon, Frank Ham, Rene Pecnik, and Heinz Pitsch. A flamelet-based model for supersonic combustion. *Annual research briefs*, pages 47–58, 2009.
- [21] B. Thornber, A. Mosedale, D. Drikakis, D. Youngs, and R.J.R. Williams. An improved reconstruction method for compressible flows with low mach number features. *Journal of Computational Physics*, 227(10):4873 – 4894, 2008.
- [22] V.P. Zhukov and A.F. Kong. Development of a skeletal kinetic mechanism of methane oxidation for high pressures and temperatures. In *Proceedings of the Space Propulsion Conference, Rome*, 2016.